

Article

Cerium Oxide/Graphene Oxide Hybrid: Synthesis, Characterization, and Evaluation of Anticancer Activity in a Breast Cancer Cell Line (MCF-7)

J. Saranya ^{1,*}, P. Saminathan ², Seshadri Reddy Ankireddy ³, Mohammed Rafi Shaik ^{4,*}, Mujeeb Khan ⁴, Merajuddin Khan ⁴ and Baji Shaik ⁵

¹ Department of Electronics and Communication Engineering, Rajalakshmi Engineering College, Chennai 602105, Tamil Nadu, India

² Sasaam Biologicals Lab Services, Ashok Nagar, Chennai 600083, Tamil Nadu, India

³ Dr. Buddolla's Institute of Life Sciences, Renigunta Road, Tirupati 517503, Andhra Pradesh, India

⁴ Department of Chemistry, College of Science, King Saud University, P.O. Box 2455, Riyadh 11451, Saudi Arabia

⁵ School of Chemical Engineering, Yeungnam University, Gyeongsan 38541, Republic of Korea

* Correspondence: saranya.j@rajalakshmi.edu.in (J.S.); mrshaik@ksu.edu.sa (M.R.S.); Tel.: +966-11-4670439 (M.R.S.)

Abstract: In the present study, we used a simple ultrasonic approach to develop a Cerium oxide/Graphene oxide hybrid (CeO₂/GO hybrid) nanocomposite system. Particle size analysis, Fourier Transform Infrared Spectroscopy (FTIR), Scanning Electron Microscopy (SEM), and X-ray Diffraction (XRD) have been used to analyze the physio-chemical characteristics of the developed nanocomposite. The synthesized hybrid system has also been examined to assess its anticancer capability against MCF-7 cell lines and normal cell lines at different sample concentrations, pH values, and incubation intervals using an antiproliferative assay test. The test results demonstrate that as sample concentration rises, the apoptotic behavior of the CeO₂/GO hybrid in the MCF-7 cell line also rises. The IC₅₀ was 62.5 µg/mL after 72 h of incubation. Cytotoxicity of cisplatin bound CeO₂/GO hybrid was also tested in MCF-7 cell lines. To identify apoptosis-associated alterations of cell membranes during the process of apoptosis, a dual acridine orange/ethidium bromide (AO/EB) fluorescence staining was carried out at three specified doses (i.e., 1000 µg/mL, 250 µg/mL, and 62.5 µg/mL of CeO₂/GO hybrid). The color variations from both live (green) and dead (red) cells were examined using fluorescence microscopy under in vitro conditions. The quantitative analysis was performed using flow cytometry to identify the cell cycle at which the maximum number of MCF-7 cells had been destroyed as a result of interaction with the developed CeO₂/GO hybrid (FACS study). According to the results of the FACS investigation, the majority of cancer cells were inhibited at the R3 (G2/M) phase. Therefore, the CeO₂/GO hybrid has successfully showed enhanced anticancer efficacy against the MCF-7 cell line at the IC₅₀ concentration. According to the current study, the CeO₂/GO platform can be used as a therapeutic platform for breast cancer. The synergetic effects of the developed CeO₂/GO hybrid with the MCF-7 cell line are presented.

Keywords: CeO₂/GO hybrid; Cis-CeO₂/GO hybrid; MTT; FACS; AO/EB; MCF-7



Citation: Saranya, J.; Saminathan, P.; Ankireddy, S.R.; Shaik, M.R.; Khan, M.; Khan, M.; Shaik, B. Cerium Oxide/Graphene Oxide Hybrid: Synthesis, Characterization, and Evaluation of Anticancer Activity in a Breast Cancer Cell Line (MCF-7). *Biomedicines* **2023**, *11*, 531. <https://doi.org/10.3390/biomedicines11020531>

Academic Editor: Paola Maroni

Received: 14 January 2023

Revised: 6 February 2023

Accepted: 9 February 2023

Published: 12 February 2023



Copyright: © 2023 by the authors. Licensee MDPI, Basel, Switzerland. This article is an open access article distributed under the terms and conditions of the Creative Commons Attribution (CC BY) license (<https://creativecommons.org/licenses/by/4.0/>).

1. Introduction

As per the cancer statistics revealed by ICMR in the year 2021, India has over 200,000 new cases on average and 43,000 deaths due to breast and cervix cancer. Approximately 80% of the woman from the age group of 45 years and 43% of the woman from age group of 65 years and above were diagnosed with breast cancer. Despite the fact that it can destroy and impair organs, cancer is an aberrant or uncontrolled cellular proliferation that can invade other healthy tissues of the body. Conversely, one of the leading causes of death for women in wealthy countries today is breast cancer. Chemotherapy treatment may last for

hours, days, weeks, or even months, depending on how far radiotherapy and chemotherapy for cancer treatment have come. Radiation therapy sometimes causes tissue damage near organs [1]. Both of these treatments carry risks, are expensive, and have specific side effects. As a result, cancer requires a straightforward and effective treatment. Much emphasis has been paid to the application of nanoscience in the treatment of cancer [2,3].

Nano-sized materials, which are typically 1–100 nm, are used in medical nanotechnology. These materials are used in the design and production of medicinal medications and devices [4]. One of the main advantages of nanomaterial-based cancer therapy over free medicines is targeted delivery. Targeted delivery based on nanoparticles has recently advanced. Using either passive or active targeting, the concept of targeted delivery seeks to precisely target particular cancer cells [5]. Nanomaterials are widely used in cancer radiation therapy, immunotherapy, and combined therapy for advancing the therapy strategy. Currently, inorganic nanoparticle-based nanomaterials are increasingly being explored for a variety of medicinal applications, including as anticancer agents [6]. Among various inorganic nanoparticles, metal oxides are more favored for biomedical applications, including drug delivery, cell imaging, and cancer treatment [7]. Metallic and/or metal oxide nanoparticles demonstrate characteristic physicochemical properties including excellent optical, magnetic, and electrical activities, and so on [8]. Out of several metal oxides, iron, nickel, cerium cobalt-based oxide nanoparticles have been considerably used for several biomedical applications due to their superior optical and magnetic properties. These materials have been known to exhibit effective biological potential, such as the ability to induce DNA damage, oxidative stress, genotoxic effects, and anti-inflammatory responses. Due to these effects of metal oxide NPs, they are considered as potential therapeutic anticancer agents. In these regards, various magnetic metal and metal oxide nanoparticle (MNP) systems, have been successfully utilized in cancer treatment, which have shown significant advancements in a number of pre-clinical cancer theranostics applications [9].

For example, to diminish the excessive usage of aggressive anticancer drugs, different options are required, including the application of copper oxide (CuO) NPs, as reported by Dringen et al., who have explored the effect of uptake and toxicity of ionic copper by C6 glioma cells [10]. Besides, many other studies have suggested that a variety of magnetic NPs induce selective autophagy in cancerous cells without affecting normal cells, and thereby exhibit an intrinsic toxicity specifically toward cancer cells, which would enhance their therapeutic effect [11]. MNPs can display toxicity through mechanisms such as the production of reactive oxygen species (ROS), generation of ROS directly from the NP surface, and through alteration of mitochondria [12]. CeO₂ NPs receive a lot of attention in nanoscience because they are useful as catalysts, fuel cells, and antioxidants in biosystems [13]. In general, cerium can exist in both Ce³⁺ and Ce⁴⁺ oxidation states. The surface Ce³⁺: Ce⁴⁺ ratio is influenced by the microenvironment. As a result, the microenvironment and synthesis process are key variables in the estimate of CeO₂NPs' biological activity [14]. CeO₂NPs have reportedly recently gained popularity as attractive materials in a number of significant domains, including analysis, drug delivery, and biomedicine [15–19]. On the other hand, Carbon atoms are arranged in single layers in the two-dimensional compound called as graphene. Due to its unique physical, chemical, and mechanical properties, nano-sized graphene and its associated compounds have attracted a great deal of interest for usage in various biological applications [20,21]. Because of its high surface to volume ratio, outstanding loading capacity, and good near-infrared (NIR) absorbance, one prominent graphene derivative, graphene oxide (GO), has been widely used in biosensors, drug and gene delivery vectors, imaging contrast agents, and photothermal therapy mediators [22–27].

In addition, nanomaterials are becoming popular as drug vehicles to achieve fast-cytoplasmic drug release to cancer cells. Particularly, the lysosomal pH-triggered fast drug release nanoparticles have gained considerable attention. Since, due to their excellent physicochemical properties, including high stability and smaller size, nanomaterials, can be easily internalized through endocytosis and end up in endosomes and lysosomes, where

the pHs is approximately 5.5 (endosomes) and 5 (lysosomes) [28]. In this regard, Shen et al. have prepared cisplatin-loaded nanoparticles with pH-responsive polymeric cores, which dissolved at $\text{pH} < 6$ and are rapidly internalized and transferred to lysosomes [29]. Similarly, Gao et al. have reported that doxorubicin conjugated magnetite nanoparticles with an effective pH response have demonstrated much higher anticancer activity than free DOX [30]. In addition to pH, particle size and surface composition also influence anticancer properties, such as cellular uptake *in vitro* and whole-body transport *in vivo* [31].

According to the characterization of these cell lines, cancer cell lines are an excellent model for research into the molecular mechanisms that cause the disease. The use of cancer cell lines for research has been widespread, and they have proven to be an effective tool for the genetic approach [32]. A deeper knowledge of the unregulated genes was made possible by the use of cancer cell lines. Owing to these changes, it has been confirmed that the CeO_2 NPs were fabricated on the surface of GO NPs. Experiments in cell lines (*in vitro* tests) are not alternatives to animal tumor models (*in vivo* experiments). Experiments in cell lines are just one step in the preclinical investigation of the potential new drug, after which, *in vivo* experiments are performed in tumor bearing mice. To examine genetic, epigenetic, and cellular pathways; analyze proliferative dysregulation, apoptosis, and cancer development; establish important molecular markers; and screen and characterize cancer treatments, the appropriate *in vitro* model must be employed in cancer research [33]. Using an anti-proliferative assay, this work seeks to synthesize a CeO_2/GO nanocomposite and evaluate its anticancer potential in MCF-7 cell lines and normal cell lines. To further support the use of the developed nanoplatform as a drug delivery platform, CeO_2/GO nanocomposites were used as an anticancer agent in therapeutics.

2. Results and Discussion

2.1. XRD Analysis

The phase purity and nanocomposite crystallinity were investigated using the powder XRD analysis, as depicted in Figure 1. The results show that considerable diffraction peaks were identified 2θ at 26.4° , 29.7° , 47.3° , 57.8° , and 78.1° for the presence of the lattice planes of (111), (200), (220), (222), and (333), respectively. However, there was a small peak observed with a less intense 2θ at 19.2° , which was ascertained for the presence of a graphitic core of the GO. The degree of crystallinity and peak intensity both deteriorate when CeO_2 is deposited on the surface of GO sheets. Based on these observations, the GO platform has been used for the fabrication of the CeO_2 NPs on their surface.

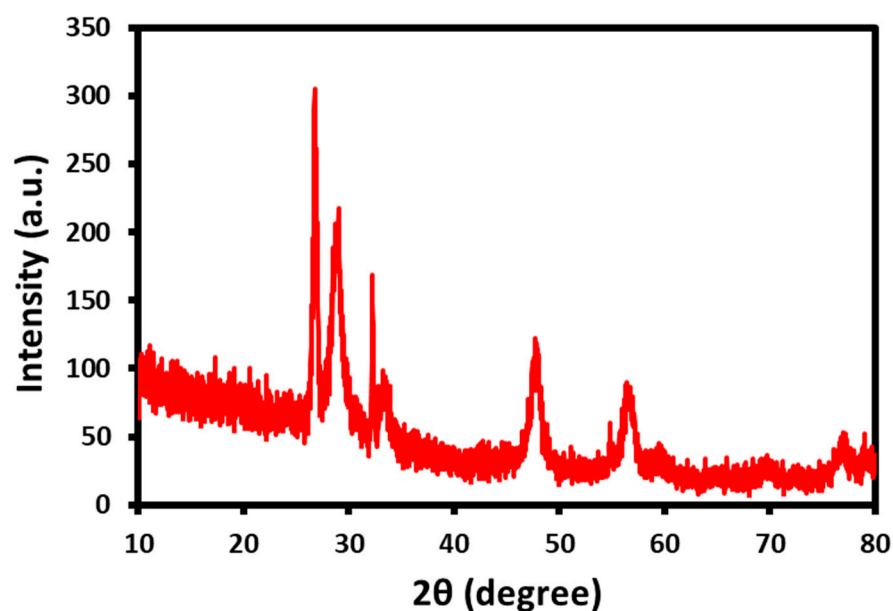


Figure 1. X-ray diffraction patterns of the CeO_2/GO nanocomposite.

2.2. UV-Visible Analysis

Initially, the authorization of the development of the GO/CeO₂ nanocomposite was examined using UV-Visible analysis (Figure 2). The UV-Vis results exhibited the absorption band of an intense surface plasmon resonance (SPR) absorption peak at 235 nm, which corresponds to $\pi-\pi^*$ transitions of the remaining sp² C=C bonds [34,35], and the another absorption peak around 300–350 nm, which corresponds to the plasma resonance of CeO₂ [36]. The ultraviolet-visible analysis clearly indicates the formation of the GO/CeO₂ nanocomposite.

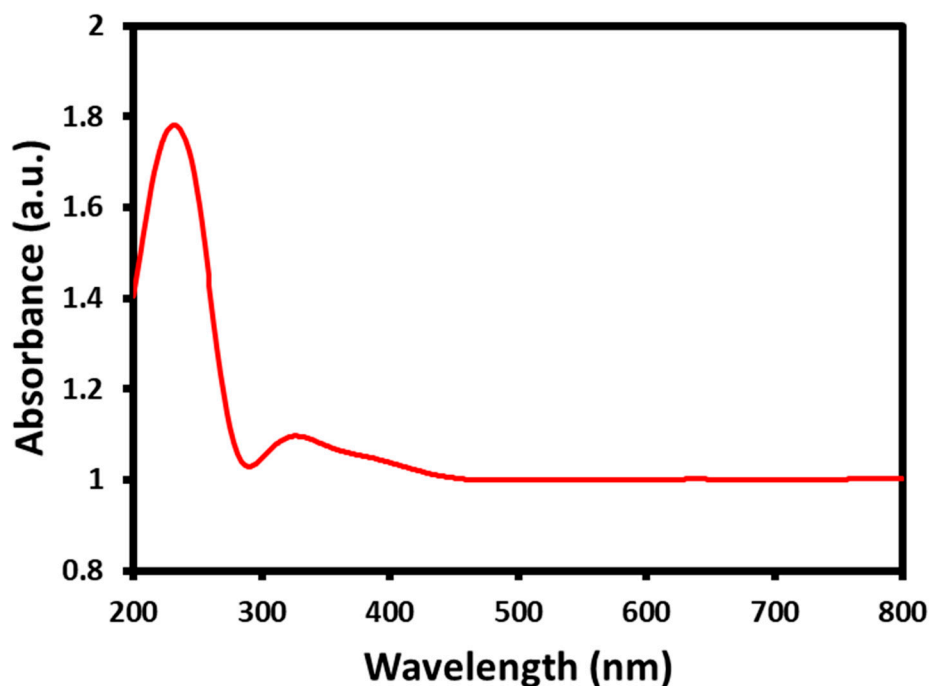


Figure 2. UV-Visible analysis of the CeO₂/GO nanocomposite.

2.3. Surface Morphology Analysis

An outstanding possibility for morphological analysis and nanocomposite size analysis is provided by SEM inspection. The typical SEM micrograph of the synthesized CeO₂/GO nanocomposite surface morphology shows irregular vesicles at the range of 50 μm at 400 \times magnification and 540 \times magnification, respectively. Further, at 850 \times magnification, cubic irregular vesicles at the size of 20 μm with detailed encapsulation of CeO₂/GO NPs were found, as shown in Figure 3. Previous studies have shown that nanoparticles without any agglomeration exhibit stable behavior because they have surface charges [37]. The hierarchical structure of the CeO₂/GO nanocomposite improves anti-cancer activity, and the same is affirmed through in vitro studies using MCF-7 cell lines and normal HeLa cells.

2.4. FT-IR Analysis

The functional group changes of CeO₂ NPs before and after treatment with GO were investigated using the FT-IR analysis, as presented in Figure 4. According to the image, several characteristic absorption peaks were observed at 3401, 1580, 1379, and 1125 cm^{-1} , which are responsible for the presence of stretching frequencies of hydroxyl, Ce-OH, bending frequencies of Ce-O, and metal oxide bonds, respectively. However, significant changes were observed in the aforementioned peaks due to the incorporation of GO. The hydroxyl and Ce-OH bending peaks were shifted to higher and lower wavenumbers, respectively. Interestingly, the bending frequency of Ce-O has increased dramatically due

to the presence of GO immobilization. Owing to these changes, it has been confirmed that the CeO_2 NPs were fabricated on the surface of CeO_2/GO NPs.

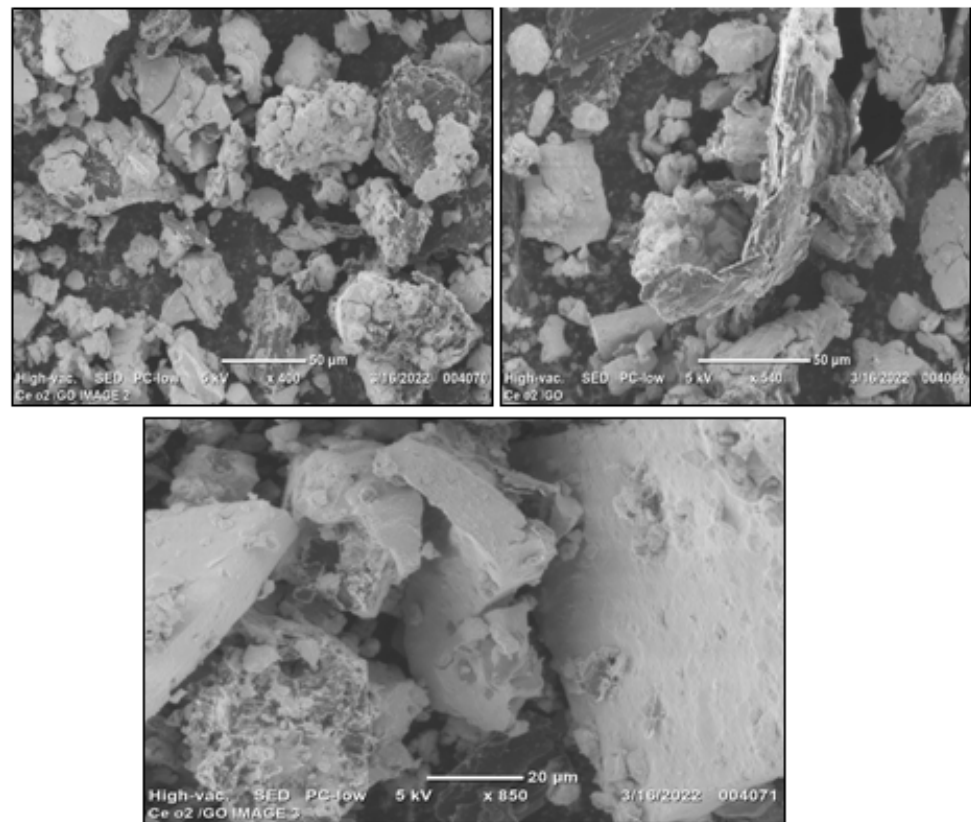


Figure 3. SEM images of the CeO_2/GO nanocomposite with a magnification of 400 \times , 540 \times , and 850 \times .

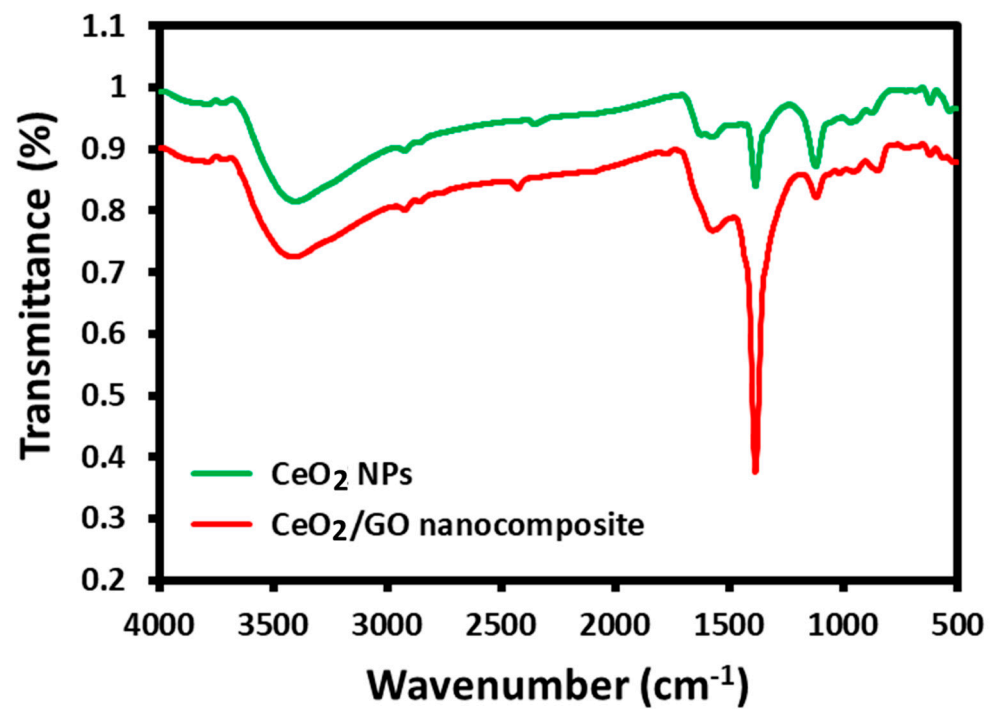


Figure 4. FT-IR analysis of CeO_2 NPs and $\text{Ce}_2\text{O}/\text{GO}$ nanocomposites.

2.5. Study of Cytotoxicity Effects of CeO₂/GO NC and Cis-CeO₂/GO NC in the MCF-7 Cell Line and Normal Cell Line Using the MTT Assay

The cytotoxicity effects of the developed CeO₂/GO nanocomposite upon interaction at various concentrations, such as 1000 µg/mL, 500 µg/mL, 250 µg/mL, 125 µg/mL, 62.5 µg/mL, and 31.2 µg/mL, with nearing 100,000 normal cells under different pH values, such as 7.2, 6, and 8.5, are presented in Figures 5–7, respectively. Further, the interaction of the CeO₂/GO nanocomposite with the MCF-7 cell line with and without cisplatin drug is presented in Figures 8 and 9.

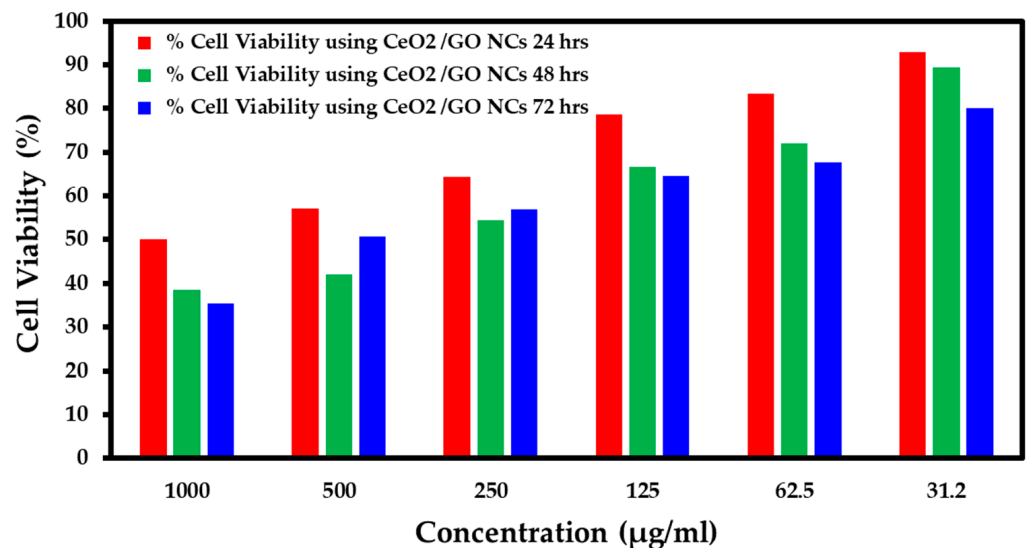


Figure 5. Percent cell viability for the normal cell line (pH 7.2).

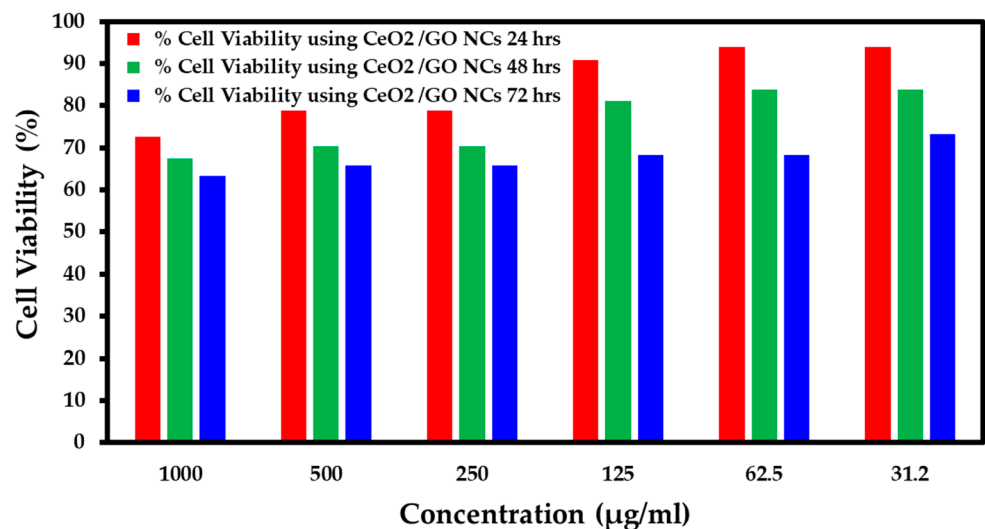


Figure 6. Percent cell viability for the normal cell line (pH 6).

During the interaction of 1000 µg/mL of CeO₂/GO with a normal cell line under pH 7.2, the % live cells was 50, under pH 6, the % live cells was 72.72, and for pH 8.5, the % live cells was 72. Similarly, when the minimum concentration of 31.2 µg/mL of the CeO₂/GO nanocomposite was combined with a normal cell line under pH 7.2, the % live cells was 92.85, under pH 6, the % live cells was 93.93, and for pH 8.5, the % live cells was 76. Based on the observation, the ideal pH condition for which the developed CeO₂/GO nanocomposite synergized well with a normal cell line and showed minimal toxicity effects (more live cells are seen) is pH 6, as shown in Figures 5–7.

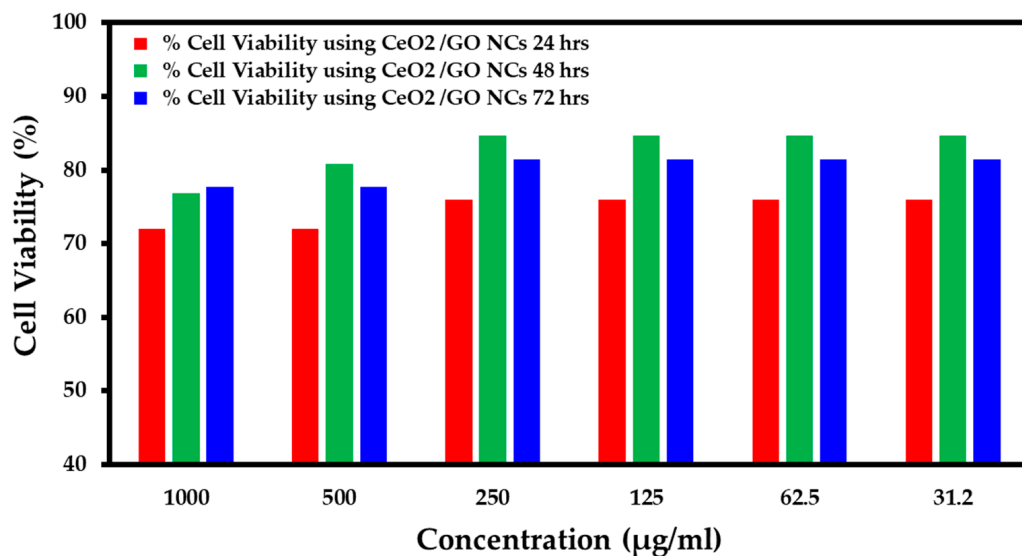


Figure 7. Percent cell viability for the normal cell line (pH 8.5).

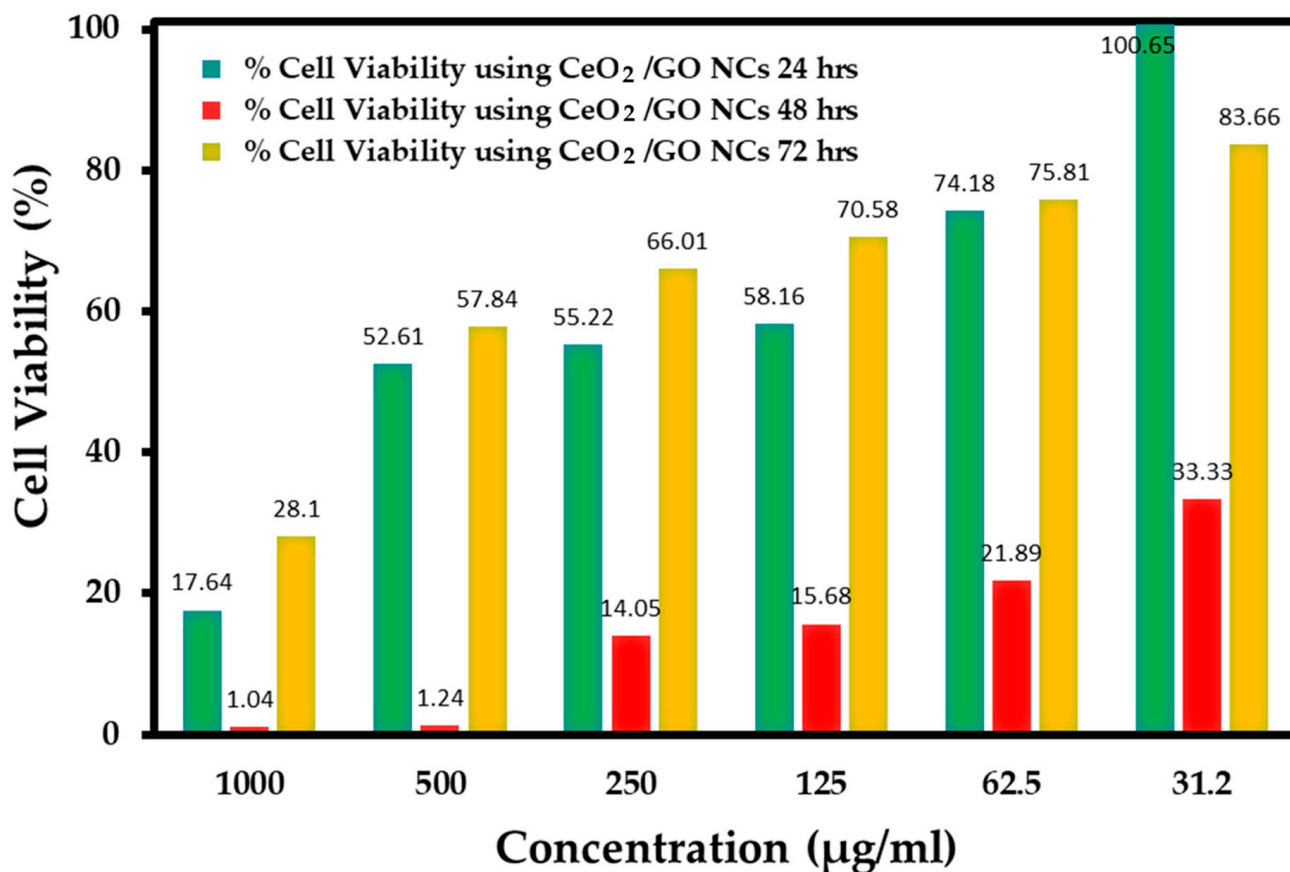


Figure 8. Percent cell viability of CeO₂/GO hybrid in the MCF-7 cell line without drug.

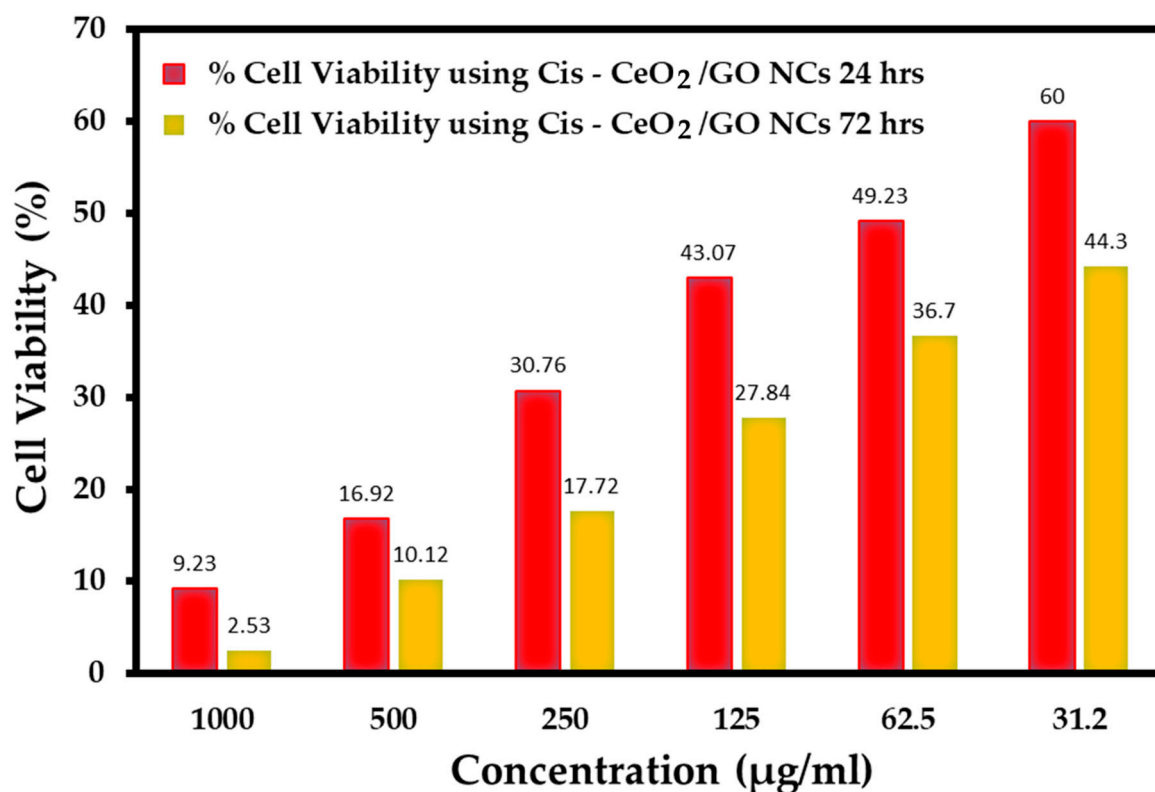


Figure 9. Percent cell viability of Cis-CeO₂/GO hybrid in the MCF-7 cell line.

The cytotoxicity effects of the developed CeO₂/GO NCs were recorded against MCF-7 cells, as shown in Figure 8. At the maximum incubation period of 72 h, when the maximum concentration of 1000 µg/mL interacted with MCF-7 cells, the % live cells recorded was 28, and at the 31.2 µg/mL concentration, the % live cells recorded was 83.66. These observations further affirm the anticancer effect of the developed CeO₂/GO nanocomposite. Further, the interaction of Cis-CeO₂/GO NCs with the MCF-7 cell line was carried out and observations were recorded at 24 and 72 h, as shown in Figure 9. For 1000 µg/mL of Cis-CeO₂/GO nanocomposite, the % live cells was 2.53, and for 31.2 µg/mL, the % live cells was 44.3. A lattice of oxygen surrounds the cerium center of cerium oxide nanoparticles (NPs) [38]. Under neutral pH conditions, these NPs act as antioxidants and cytoprotectants in healthy cells. Additionally, in an acidic solution, these NPs have prooxidant and cytotoxic effects, which is a feature of tumor cells. The anticancer effects of cerium oxide NPs were investigated *in vitro*, and the findings indicated that cerium oxide NPs suppress tumor cell proliferation [39]. Another study revealed that cerium oxide NPs with (10 µg/mL) can inhibit gastric tumor cell proliferation and reduce tumor cell migration [40]. Due to its high surface to volume ratio and the unique physicochemical characteristics of CeO₂ NPs and GO, the synthesized CeO₂/GO nanocomposite exhibit outstanding dose-dependent anticancer activity through DNA damage and the generation of reactive oxygen species (ROS). Further, Figure 9 demonstrates the increased cytotoxicity effects of Cis-CeO₂/GO NPs when added with cisplatin on the MCF-7 cell line. This affirms the effective binding of anticancer drug molecules with the CeO₂/GO hybrid.

2.6. Direct Fluorescence Microscopic Analysis of Apoptosis Induction

An acridine orange/ethidium bromide (AO/EB) dual stain study was performed to detect the presence of live and dead cells using fluorescence emission under an *in vitro* microenvironment. The cells were fixed in a 3:1 ratio of ethanol and phosphate buffer solution (PBS) for 1 h at room temperature. The cells treated with the CeO₂/GO hybrid nanocomposite were labeled with a 1:1 ratio of AO and EB in PBS and were incubated.

Then, the excess unbinding dye was removed by washing with PBS and the stained cells were visualized using a fluorescence microscope, as shown in Figure 10.

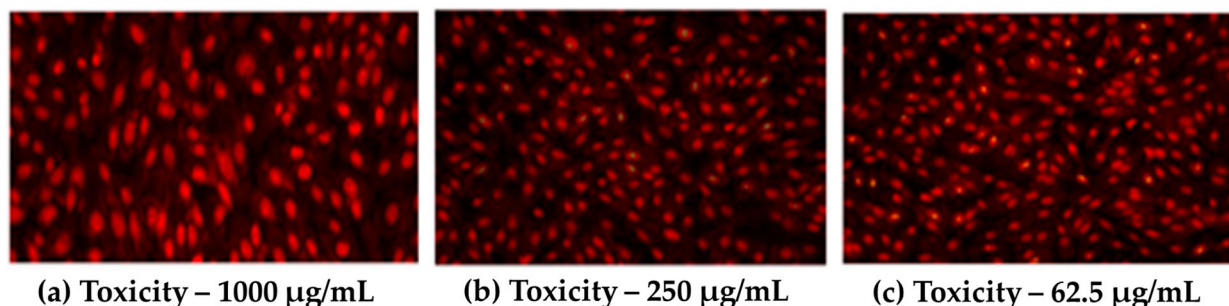


Figure 10. Microscopic fluorescent images of (a) MCF-7 cells with 1000 µg/mL CeO₂/GO hybrid, (b,c) MCF-7 cells with 250 µg/mL and 62.5 µg/mL concentrations of CeO₂/GO hybrid complexes, respectively.

To identify the presence of live and dead cells using fluorescence emission in an *in vitro* microenvironment, a dual stain analysis employing acridine orange/ethidium bromide (AO/EB) dyes were conducted. For 1 h at room temperature, the cells were fixed in a 3:1 mixture of ethanol and phosphate buffer solution (PBS). After being treated with the CeO₂/GO hybrid nanocomposite, the cells were incubated with AO and EB in a 1:1 ratio in PBS. Following a PBS wash to remove any excess unbinding dye, stained cells were viewed under a fluorescence microscope, as shown in Figure 10.

These pictures showcase the morphological alterations and color emission variations that result from mixing acridine orange (AO) and ethidium bromide (EB) dyes in an *in vitro* environment. More dead cells are shown in Figure 10a, and they appear red because they can absorb the ethidium bromide (EB) dye by itself. This affirms the apoptotic behavior of the developed CeO₂/GO NCs. Figure 10b,c shows the coexistence of living and dead cells as a result of the live cells' uptake of the acridine orange (AO) dye and the dead cells' uptake of the ethidium bromide (EB) dye. This study demonstrates the morphological changes that cell lines experienced when they interact with different CeO₂/GO NC concentrations.

2.7. Cell Cycle Analysis

This study aims to determine the phase cycle at which the majority of cancer cells were destroyed. Figure 11 shows the apoptotic behavior of a produced CeO₂/GO hybrid at two different concentrations (62.5 µg/mL and 31.2 µg/mL).

Figure 11a represents untreated MCF-7 cells with a total of 3032 cells, which were subject to cell cycle analysis. In phase 1, almost 5% of cancerous cells were dead, in phase 2, 66% of cancerous cells were dead, and in phase 3, 91.49% of cells were dead. The cell death recorded here is an outcome of the apoptotic behavior of cancer cells. Figure 11b represents recordings from cell cycle analysis of a total of 10,000 MCF-7 cells, which were synergized with 62.5 µg/mL of CeO₂/GO NCs. Here, the second cell cycle, which only contains 3854 living cells, records the highest levels of apoptotic behavior. Figure 11c represents treated HeLa cells with a total of 1022 cells, which were subject to cell cycle analysis. Upon interaction of MCF-7 cells with 31.2 µg/mL, maximum cell cycle arrest was found in cell cycle 2. Cell death rate is more effective in phase 2 rather in the rest of the phases, and the same further confirms the anticancer properties of the developed CeO₂/GO nanoplatform.

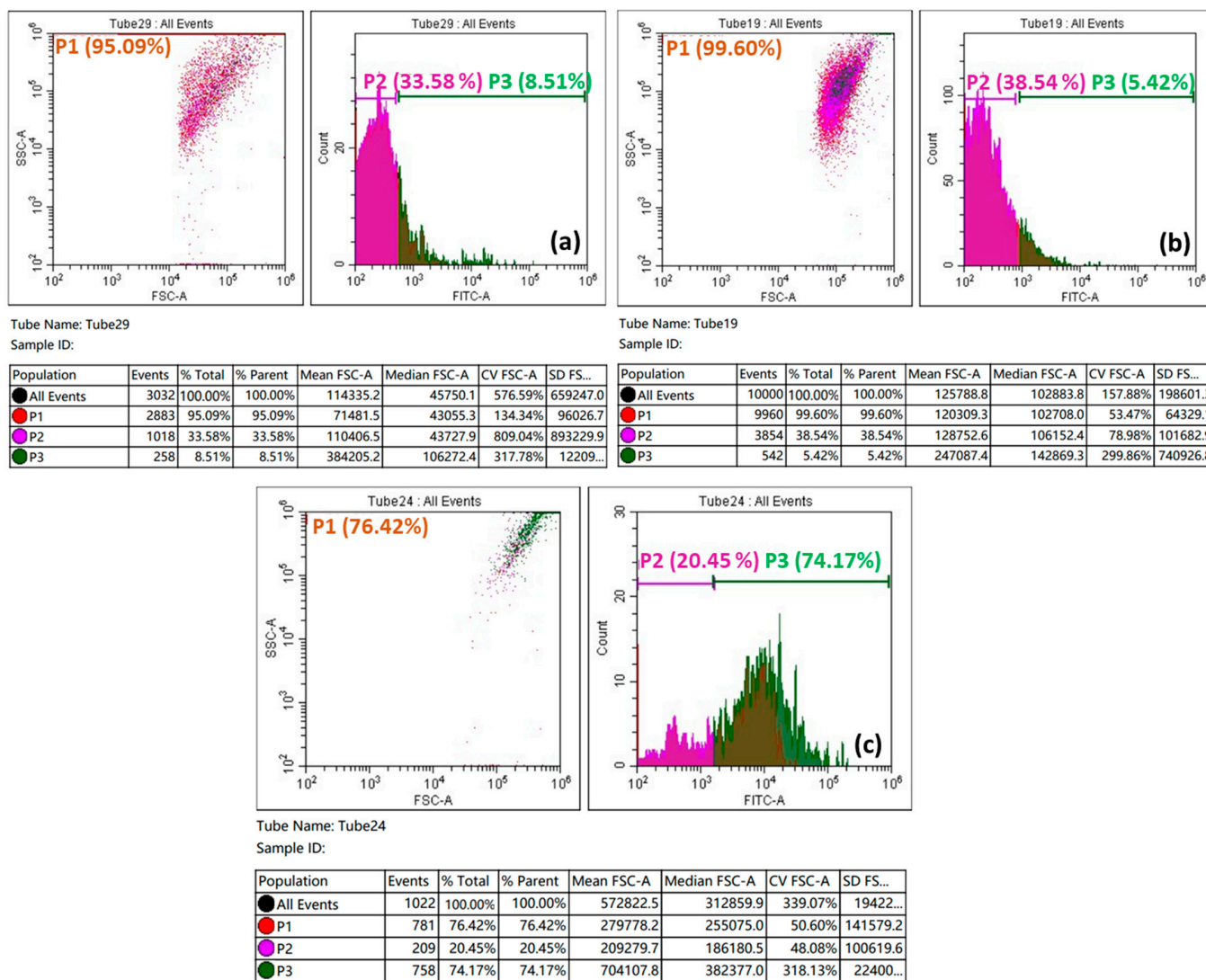


Figure 11. Flowcytometry of (a) untreated MCF-7 cells, and (b,c) treated MCF-7 cells with 62.5 µg/mL and 31.2 µg/mL concentrations of CeO₂/GO hybrid complexes.

3. Materials and Methods

3.1. Materials

All chemicals and solvents utilized in this inquiry were of the highest purity and quality for analysis. Sodium hydroxide (NaOH) and cerous nitrate hexahydrate (CeN₃O₉·6H₂O) were bought from Fischer Scientific, Mumbai, India. Utilizing the RIGAKU micro flux 2C, Tokyo, Japan, the X-ray Diffraction (XRD) spectrum of the CeO₂/GO hybrid nanosystem was captured. A PerkinElmer lambda 35 (Waltham, MA, USA) UV/Vis spectrophotometer was used for the optical measurements. Using Scanning Electron Microscopy (SEM) produced by TESPON, Tokyo, Japan, surface morphology was determined. Particle size analysis was done using the Horiba-Particle Analyzer. A spectrophotometer was used to capture the absorption spectra (Labman scientific instruments, Chennai, India). Confocal images of HeLa cells were obtained using a Metzer Inverted confocal microscope, Mumbai, India.

3.2. Preparation of Cerium Oxide Nanoparticles (CeO₂NPs)

A cost-effective wet chemical method was used to synthesize cerium oxide nanoparticles (CeO₂ NPs) at room temperature. The first step was to dissolve 0.1 M of cerous nitrate hexahydrate (CeN₃O₉·6H₂O) in 100 mL of pure water. The resulting 100 mL cerous

nitrate hexa hydrate solution was then mixed with 50 mL of 0.5 M sodium hydroxide (NaOH) solution. The resultant solution was kept under constant stirring for 2 h and color change was detected. Further stirring was done until a yellowish solution appeared, confirming the presence of CeO₂ NPs. This yellowish solution was set aside to allow the CeO₂ nanoparticles to settle before being rinsed three times with distilled water. It was then annealed at 350 °C and dried at 150 °C. The powder that was so obtained was put to use for other analytical tasks.

3.3. Preparation of Graphene Oxide (GO)

Graphite powder (2 g) was added to concentrated H₂SO₄ (46 mL) at 0 °C in an ice bath and stirred for 5 min. NaNO₃ (1 g) was then added and the solution was stirred for 5 min. KMnO₄ (6 g) was added slowly into the resulting mixture and stirring continued for 30 min at 35 °C. H₂O (96 mL) was then added dropwise to the above mixture and the temperature was increased to 98 °C and maintained for 30 min; then, a further aliquot of H₂O (280 mL) was added and stirring was continued for 10 min. Finally, aqueous H₂O₂ (30 mL, 30%) was added dropwise [37].

3.4. Preparation of CeO₂/GO Nanocomposite

We used 100 mL of distilled water to dilute 1 g of prepared CeO₂ NPs powder before it was ultrasonically processed for 30 min. Following that, 0.25 g of graphene oxide (GO) was diluted in 50 mL of distilled water and subjected to 2 h of ultrasonication. To create a nanocomposite solution, the two solutions containing the mixture are finally blended. Additionally, the combinations underwent two hours of stirring after being combined in order to produce a homogenous solution. After allowing the materials to settle, they were three times washed with distilled water to produce CeO₂/GO NCs.

3.5. Preparation of Cis-CeO₂/GO Hybrid Nanocomposite

At first, 1000 µg/mL of cisplatin were added to a well containing HeLa cell line. Then for each of the eight concentrations (7.8, 15.6, 31.2, 62.5, 125, 250, 500, and 1000 µg/mL) half of the concentration will be (CeO₂/GO) sample and rest half will be cisplatin (for instance, 500 µg/mL of cisplatin and 500 µg/mL of CeO₂/GO are present in a 1000 µg/mL stock solution). The same steps are repeated for additional concentrations. The Cis-CeO₂/GO hybrid was developed using the aforementioned process, and it was then subject to an MTT assay routine to estimate the % cell viability.

3.6. Cytotoxicity Studies

3.6.1. Cell Lines

The Veterinary College in Vepery, Chennai provided the MCF-7 cell line. The cells were kept alive at 37 °C in a humidified atmosphere of 50 µg/mL CO₂ in Minimal Essential Medium (MEM) supplemented with 10% FBS, penicillin (100 U/mL), and streptomycin (100 µg/mL).

3.6.2. Reagents

MEM was acquired from Hi Media Laboratories, Fetal Bovine Serum (FBS) from Cistron Laboratories, Coimbatore, Tamil Nadu, Inida and Trypsin, Methylthiazolyldiphenyl-tetrazoliumbromide (MTT), and Dimethyl Sulfoxide (DMSO) from Sisco Research Laboratory Chemicals, Mumbai, India. Other chemicals and reagents were obtained from Sigma-Aldrich, Mumbai, India.

3.6.3. Evaluation of the Anticancer Activity of the CeO₂/GO Hybrid and Cis-CeO₂/GO Hybrid

The procedure incorporated for evaluation of the CeO₂/GO hybrid and Cis-CeO₂/GO hybrid are presented in supplementary sections. The UV Spectrophotometer was used

to measure the absorbance at 570 nm. The following formula was used to determine the percentage of viable cells:

$$\% \text{ cell viability} = \text{Optical density of treated cells} / \text{Optical density of control cells} \times 100$$

Each assay includes a cell control and sample control to provide a comprehensive evaluation of cell viability and the same were plotted as graphs by taking the concentration of the sample on the X-axis and the % cell viability on the Y-axis.

3.7. Dual Staining (Acridine Orange and Ethidium Bromide Staining)

Acridine orange can stain both living and dead cells. Ethidium bromide only stains cells that have lost the integrity of their membranes. Cells that are alive will be green. As a result of chromatin condensation and nuclear fragmentation, early apoptotic cells will stain green and have brilliant green spots in their nuclei. In addition to incorporating ethidium bromide and staining orange, late apoptotic cells also exhibit contracted and typically broken nuclei in contrast to necrotic cells.

3.8. Flow Cytometry Study

Cell cycle arrest was investigated using a protocol [29], and the experimental procedure is provided under the supplementary section. The flow cytometer was used to examine the cell phase distribution in the labeled cells.

4. Conclusions

In conclusion, a CeO₂/GO hybrid nanocomposite has been developed using an easy and affordable ultrasonic technique. The physio-chemical characteristics were examined using analysis tools such as XRD, Particle Size Analysis, SEM, and FTIR. Scanning electron microscopy was utilized to confirm the surface morphology (SEM). The particle size of the developed CeO₂/GO hybrid nanocomposite was found to be 68.94 μm on average, which results in a high surface to volume ratio and improved anticancer efficacy in the MCF-7 cell line. The obtained CeO₂/GO hybrid was subject to qualitative analysis, such as the MTT assay and dual stain study. The outcome of this study resulted in the identification of effective anticancer properties at the 62.5 μg/mL CeO₂/GO hybrid concentration. To determine the cell cycle phase at which the majority of cancer cells were arrested, quantitative analysis (FACS) was performed on three sets of CeO₂/GO concentrations, including the IC₅₀ concentration. In comparison with the Cis-CeO₂/GO hybrid, the CeO₂/GO hybrid is superior. The reason behind is that at t = 24 h and at IC₅₀ 62.5 μg/mL, the % cell viability is 21.89 for the CeO₂/GO hybrid and 36.7 for the Cis-CeO₂/GO hybrid. Maximum % cell inhibition is recorded for the CeO₂/GO hybrid. This work primarily focuses on the assessment of the cytotoxic behavior of the CeO₂/GO hybrid on MCF-7 cells under in vitro conditions. Based on the results from in vitro studies, the prepared CeO₂/GO hybrid can be used as a theranostic platform for breast cancer. Thus, for future work, the developed CeO₂/GO hybrid can be a potential subject for in vivo analysis and clinical trials for further confirmation and proceedings.

Author Contributions: Conceptualization, J.S.; methodology, J.S.; software, P.S. and S.R.A.; validation, J.S., P.S. and S.R.A.; formal analysis, M.K. (Mujeeb Khan), M.K. (Merajuddin Khan) and B.S.; investigation, J.S., P.S., S.R.A. and M.R.S.; resources, J.S. and M.R.S.; data curation, J.S., P.S., S.R.A., M.R.S. and M.K. (Mujeeb Khan); writing—original draft preparation, J.S., P.S., S.R.A. and M.R.S.; writing—review and editing, M.R.S.; visualization, J.S.; supervision, J.S.; project administration, J.S.; funding acquisition, M.R.S. All authors have read and agreed to the published version of the manuscript.

Funding: Researchers Supporting Project number (RSPD2023R665), King Saud University, Riyadh, Saudi Arabia.

Institutional Review Board Statement: Not applicable.

Informed Consent Statement: Not applicable.

Data Availability Statement: Data contained within the article.

Acknowledgments: The authors acknowledge the funding from Researchers Supporting Project number (RSPD2023R665), King Saud University, Riyadh, Saudi Arabia.

Conflicts of Interest: The authors declare no conflict of interest.

References

1. Baumann, M.; Krause, M.; Overgaard, J.; Debus, J.; Bentzen, S.M.; Daartz, J.; Richter, C.; Zips, D.; Bortfeld, T. Radiation oncology in the era of precision medicine. *Nat. Rev. Cancer* **2016**, *16*, 234–249. [[CrossRef](#)] [[PubMed](#)]
2. Sridharan, M.; Kamaraj, P.; Arockiaselvi, J.; Pushpamalini, T.; Vivekanand, P.; Kumar, S.H. Synthesis, characterization and evaluation of biosynthesized Cerium oxide nanoparticle for its anticancer activity on breast cancer cell (MCF 7). *Mater. Today Proc.* **2021**, *36*, 914–919. [[CrossRef](#)]
3. Kher, C.; Kumar, S. The application of nanotechnology and nanomaterials in cancer diagnosis and treatment: A review. *Cureus* **2022**, *14*, e29059. [[CrossRef](#)]
4. Cheng, Z.; Li, M.; Dey, R.; Chen, Y. Nanomaterials for cancer therapy: Current progress and perspectives. *J. Hematol. Oncol.* **2021**, *14*, 1–27. [[CrossRef](#)] [[PubMed](#)]
5. Ali, E.S.; Sharker, S.M.; Islam, M.T.; Khan, I.N.; Shaw, S.; Rahman, M.A.; Uddin, S.J.; Shill, M.C.; Rehman, S.; Das, N. Targeting cancer cells with nanotherapeutics and nanodiagnostics: Current status and future perspectives. In *Proceedings of Seminars in Cancer Biology*; Elsevier, Amsterdam, The Netherlands, pp. 52–68.
6. Vinardell, M.P.; Mitjans, M. Antitumor activities of metal oxide nanoparticles. *Nanomaterials* **2015**, *5*, 1004–1021. [[CrossRef](#)]
7. Vinardell, M.; Mitjans, M. Metal/metal oxide nanoparticles for cancer therapy. *Nanooncol. Eng. Nanomater. Cancer Ther. Diagn.* **2018**, 341–364.
8. Soetaert, F.; Korangath, P.; Serantes, D.; Fiering, S.; Ivkov, R. Cancer therapy with iron oxide nanoparticles: Agents of thermal and immune therapies. *Adv. Drug Deliv. Rev.* **2020**, *163*, 65–83. [[CrossRef](#)]
9. Mukherjee, S.; Liang, L.; Veisheh, O. Recent advancements of magnetic nanomaterials in cancer therapy. *Pharmaceutics* **2020**, *12*, 147. [[CrossRef](#)]
10. Bulcke, F.; Santofimia-Castaño, P.; Gonzalez-Mateos, A.; Dringen, R. Modulation of copper accumulation and copper-induced toxicity by antioxidants and copper chelators in cultured primary brain astrocytes. *J. Trace Elem. Med. Biol.* **2015**, *32*, 168–176. [[CrossRef](#)]
11. Peynshaert, K.; Manshian, B.B.; Joris, F.; Braeckmans, K.; De Smedt, S.C.; Demeester, J.; Soenen, S.J. Exploiting intrinsic nanoparticle toxicity: The pros and cons of nanoparticle-induced autophagy in biomedical research. *Chem. Rev.* **2014**, *114*, 7581–7609. [[CrossRef](#)]
12. Reddy, L.H.; Arias, J.L.; Nicolas, J.; Couvreur, P. Magnetic nanoparticles: Design and characterization, toxicity and biocompatibility, pharmaceutical and biomedical applications. *Chem. Rev.* **2012**, *112*, 5818–5878. [[CrossRef](#)] [[PubMed](#)]
13. Gagnon, J.; Fromm, K.M. Toxicity and protective effects of cerium oxide nanoparticles (nanoceria) depending on their preparation method, particle size, cell type, and exposure route. *Eur. J. Inorg. Chem.* **2015**, *2015*, 4510–4517. [[CrossRef](#)]
14. Charbgo, F.; Ramezani, M.; Darroudi, M. Bio-sensing applications of cerium oxide nanoparticles: Advantages and disadvantages. *Biosens. Bioelectron.* **2017**, *96*, 33–43. [[CrossRef](#)] [[PubMed](#)]
15. Zhang, Y.; Wu, X.; Hou, C.; Shang, K.; Yang, K.; Tian, Z.; Pei, Z.; Qu, Y.; Pei, Y. Dual-responsive dithio-polydopamine coated porous CeO₂ nanorods for targeted and synergistic drug delivery. *Int. J. Nanomed.* **2018**, *13*, 2161. [[CrossRef](#)]
16. Popov, A.L.; Popova, N.; Gould, D.J.; Shcherbakov, A.B.; Sukhorukov, G.B.; Ivanov, V.K. Ceria nanoparticles-decorated microcapsules as a smart drug delivery/protective system: Protection of encapsulated *P. pyralis* luciferase. *ACS Appl. Mater. Interfaces* **2018**, *10*, 14367–14377. [[CrossRef](#)]
17. Asati, A.; Kaittanis, C.; Santra, S.; Perez, J.M. pH-tunable oxidase-like activity of cerium oxide nanoparticles achieving sensitive fluorogenic detection of cancer biomarkers at neutral pH. *Anal. Chem.* **2011**, *83*, 2547–2553. [[CrossRef](#)]
18. Kaittanis, C.; Santra, S.; Asati, A.; Perez, J.M. A cerium oxide nanoparticle-based device for the detection of chronic inflammation via optical and magnetic resonance imaging. *Nanoscale* **2012**, *4*, 2117–2123. [[CrossRef](#)]
19. Dhall, A.; Self, W. Cerium oxide nanoparticles: A brief review of their synthesis methods and biomedical applications. *Antioxidants* **2018**, *7*, 97. [[CrossRef](#)]
20. Syama, S.; Mohanan, P. Safety and biocompatibility of graphene: A new generation nanomaterial for biomedical application. *Int. J. Biol. Macromol.* **2016**, *86*, 546–555. [[CrossRef](#)]
21. Zhou, X.; Liang, F. Application of graphene/graphene oxide in biomedicine and biotechnology. *Curr. Med. Chem.* **2014**, *21*, 855–869. [[CrossRef](#)]
22. Hong, H.; Yang, K.; Zhang, Y.; Engle, J.W.; Feng, L.; Yang, Y.; Nayak, T.R.; Goel, S.; Bean, J.; Theuer, C.P. In vivo targeting and imaging of tumor vasculature with radiolabeled, antibody-conjugated nanographene. *ACS Nano* **2012**, *6*, 2361–2370. [[CrossRef](#)] [[PubMed](#)]

23. Chen, J.; Badioli, M.; Alonso-González, P.; Thongrattanasiri, S.; Huth, F.; Osmond, J.; Spasenović, M.; Centeno, A.; Pesquera, A.; Godignon, P. Optical nano-imaging of gate-tunable graphene plasmons. *Nature* **2012**, *487*, 77–81. [[CrossRef](#)]
24. Hong, H.; Zhang, Y.; Engle, J.W.; Nayak, T.R.; Theuer, C.P.; Nickles, R.J.; Barnhart, T.E.; Cai, W. In vivo targeting and positron emission tomography imaging of tumor vasculature with ⁶⁶Ga-labeled nano-graphene. *Biomaterials* **2012**, *33*, 4147–4156. [[CrossRef](#)]
25. Rong, P.; Yang, K.; Srivastan, A.; Kiesewetter, D.O.; Yue, X.; Wang, F.; Nie, L.; Bhirde, A.; Wang, Z.; Liu, Z. Photosensitizer loaded nano-graphene for multimodality imaging guided tumor photodynamic therapy. *Theranostics* **2014**, *4*, 229. [[CrossRef](#)] [[PubMed](#)]
26. Khan, H.A.; Lee, Y.-K.; Shaik, M.R.; Alrashood, S.T.; Ekhzaimy, A.A. Nanocomposites of Nitrogen-Doped Graphene Oxide and Manganese Oxide for Photodynamic Therapy and Magnetic Resonance Imaging. *Int. J. Mol. Sci.* **2022**, *23*, 15087. [[CrossRef](#)]
27. Adil, S.F.; Shaik, M.R.; Nasr, F.A.; Alqahtani, A.S.; Ahmed, M.Z.; Qamar, W.; Kuniyil, M.; Almutairi, A.; Alwarthan, A.; Siddiqui, M.R.H. Enhanced apoptosis by functionalized highly reduced graphene oxide and gold nanocomposites in MCF-7 breast cancer cells. *ACS Omega* **2021**, *6*, 15147–15155. [[CrossRef](#)] [[PubMed](#)]
28. González-Urías, A.; Manzanares-Guevara, L.A.; Licea-Claveríe, Á.; Ochoa-Terán, A.; Licea-Navarro, A.F.; Bernaldez-Sarabia, J.; Zapata-González, I. Stimuli responsive nanogels with intrinsic fluorescence: Promising nanovehicles for controlled drug delivery and cell internalization detection in diverse cancer cell lines. *Eur. Polym. J.* **2021**, *144*, 110200. [[CrossRef](#)]
29. Xu, P.; Van Kirk, E.A.; Murdoch, W.J.; Zhan, Y.; Isaak, D.D.; Radosz, M.; Shen, Y. Anticancer efficacies of cisplatin-releasing pH-responsive nanoparticles. *Biomacromolecules* **2006**, *7*, 829–835. [[CrossRef](#)] [[PubMed](#)]
30. Zhao, Z.; Huang, D.; Yin, Z.; Chi, X.; Wang, X.; Gao, J. Magnetite nanoparticles as smart carriers to manipulate the cytotoxicity of anticancer drugs: Magnetic control and pH-responsive release. *J. Mater. Chem.* **2012**, *22*, 15717–15725. [[CrossRef](#)]
31. Lee, H.; Fonge, H.; Hoang, B.; Reilly, R.M.; Allen, C. The effects of particle size and molecular targeting on the intratumoral and subcellular distribution of polymeric nanoparticles. *Mol. Pharm.* **2010**, *7*, 1195–1208. [[CrossRef](#)]
32. Ben-David, U.; Siranosian, B.; Ha, G.; Tang, H.; Oren, Y.; Hinohara, K.; Strathdee, C.A.; Dempster, J.; Lyons, N.J.; Burns, R. Genetic and transcriptional evolution alters cancer cell line drug response. *Nature* **2018**, *560*, 325–330. [[CrossRef](#)] [[PubMed](#)]
33. Watson, M.B.; Lind, M.J.; Cawkwell, L. Establishment of in-vitro models of chemotherapy resistance. *Anti-Cancer Drugs* **2007**, *18*, 749–754. [[CrossRef](#)]
34. Khan, M.; Al-Marri, A.H.; Khan, M.; Mohri, N.; Adil, S.F.; Al-Warthan, A.; Siddiqui, M.R.H.; Alkhatlan, H.Z.; Berger, R.; Tremel, W. Pulicaria glutinosa plant extract: A green and eco-friendly reducing agent for the preparation of highly reduced graphene oxide. *RSC Adv.* **2014**, *4*, 24119–24125. [[CrossRef](#)]
35. Johra, F.T.; Lee, J.-W.; Jung, W.-G. Facile and safe graphene preparation on solution based platform. *J. Ind. Eng. Chem.* **2014**, *20*, 2883–2887. [[CrossRef](#)]
36. Anand, K.; Murugan, V.; Mohana Roopan, S.; Surendra, T.V.; Chaturgoon, A.A.; Muniyasamy, S. Degradation treatment of 4-nitrophenol by Moringa oleifera synthesised GO-CeO₂ nanoparticles as catalyst. *J. Inorg. Organomet. Polym. Mater.* **2018**, *28*, 2241–2248. [[CrossRef](#)]
37. Saranya, J.; Sreeja, B.; Padmalaya, G.; Radha, S.; Manikandan, T. Ultrasonic assisted cerium oxide/graphene oxide hybrid: Preparation, anti-proliferative, apoptotic induction and G2/M cell cycle arrest in HeLa cell lines. *J. Inorg. Organomet. Polym. Mater.* **2020**, *30*, 2666–2676. [[CrossRef](#)]
38. Walkey, C.; Das, S.; Seal, S.; Erlichman, J.; Heckman, K.; Ghibelli, L.; Traversa, E.; McGinnis, J.F.; Self, W.T. Catalytic properties and biomedical applications of cerium oxide nanoparticles. *Environ. Sci. Nano* **2015**, *2*, 33–53. [[CrossRef](#)]
39. Pešić, M.; Podolski-Renić, A.; Stojković, S.; Matović, B.; Zmejkoski, D.; Kojić, V.; Bogdanović, G.; Pavićević, A.; Mojović, M.; Savić, A. Anti-cancer effects of cerium oxide nanoparticles and its intracellular redox activity. *Chem.-Biol. Interact.* **2015**, *232*, 85–93. [[CrossRef](#)] [[PubMed](#)]
40. Xiao, Y.-F.; Li, J.-M.; Wang, S.-M.; Yong, X.; Tang, B.; Jie, M.-M.; Dong, H.; Yang, X.-C.; Yang, S.-M. Cerium oxide nanoparticles inhibit the migration and proliferation of gastric cancer by increasing DHX15 expression. *Int. J. Nanomed.* **2016**, *11*, 3023.

Disclaimer/Publisher’s Note: The statements, opinions and data contained in all publications are solely those of the individual author(s) and contributor(s) and not of MDPI and/or the editor(s). MDPI and/or the editor(s) disclaim responsibility for any injury to people or property resulting from any ideas, methods, instructions or products referred to in the content.